

# Page Curve of Effective Hawking Radiation

---

**Chia-Jui Chou<sup>a</sup>, Hans B. Lao<sup>a</sup>, Yi Yang<sup>a,b,c</sup>**

<sup>a</sup>*Department of Electrophysics, National Yang Ming Chiao Tung University, Hsinchu, ROC*

<sup>b</sup>*Center for Theoretical and Computational Physics, National Yang Ming Chiao Tung University, Hsinchu, ROC*

<sup>c</sup>*National Center for Theoretical Physics, ROC*

*E-mail:* [chiajui.chou@nycu.edu.tw](mailto:chiajui.chou@nycu.edu.tw), [hanslao.ep07g@nctu.edu.tw](mailto:hanslao.ep07g@nctu.edu.tw),  
[yiyang@mail.nctu.edu.tw](mailto:yiyang@mail.nctu.edu.tw)

**ABSTRACT:** We study the generalized entanglement entropy in the higher dimensional two-sided eternal black hole by double holography. By introducing a moving ETW brane, which defines the effective Hawking radiation region, we find a new type of Ryu-Takayanagi surface besides the Hartman-Maldacena surface and the island Ryu-Takayanagi surface known previously. We study the phase transition among the three Ryu-Takayanagi surfaces at different temperatures and obtain the phase diagram as well as the Page curve.

---

## Contents

<b>1</b>	<b>Introduction</b>	<b>1</b>
<b>2</b>	<b>Background and Setup</b>	<b>4</b>
2.1	Generalized Entanglement Entropy	4
2.2	Black Hole Coupled to Thermal Bath	5
2.3	Double Holography	8
2.4	Brief Review of Black Hole Solution in BCFT	10
<b>3</b>	<b>Holographic Entanglement Entropy of Hawking Radiation</b>	<b>11</b>
3.1	Hartman-Maldacena Surface	13
3.2	Boundary RT Surface	15
3.3	Island RT Surface	17
<b>4</b>	<b>Phase Transitions and Page Curve</b>	<b>18</b>
4.1	Phase Transitions	18
4.2	Page Curve	21
4.3	Phase Diagram	23
<b>5</b>	<b>Conclusion</b>	<b>24</b>

---

## 1 Introduction

The calculations of Hawking showed that black holes have thermodynamic properties like temperature and entropy. The idea is that a pair production that occurs near the horizon could lead to one particle to fall into the black hole and the other to escape to infinity, this leads to the well known Hawking radiation [1, 2]. Since a black hole is formed from a pure state, this state should evolve in a way that it ends up in a final state that is also pure if the evolution were to obey unitarity. However, as the black hole evaporates completely, all that is left is thermal radiation so that the final state is in a mixed state. Apparently, the information that fell into the black hole vanishes. This leads to the black hole information paradox and violates unitarity which is one of the fundamental principle of quantum mechanics.

Don Page showed that if a black hole is formed from a pure state and evaporates unitarily then the von Neumann entropy of Hawking radiation should initially rise until the so-called Page time when it starts to drop down to zero as the black hole completely vanishes. This corresponds to the process where information can leak out from the black hole and is encoded in the Hawking radiation. However, this can only happen at late times past the Page time when the black hole has evaporated around half of its original state. This trend followed by the Hawking radiation is called the Page curve [3]. Over the years, there were many proposals in addressing the black hole information paradox [4–12]. It was believed that the Page curve can only be obtained in the quantum gravity theory.

It has been shown by Bekenstein and Hawking that the entropy of a black hole is proportional to its horizon area which is the so-called Bekenstein-Hawking (BH) formula [13, 14]. This is a clear demonstration of the connection between a quantum-mechanical quantity and a geometric quantity. This connection was later generalized by Ryu and Takayanagi through the AdS/CFT correspondence, where they proposed a prescription connecting the entanglement entropy of a region  $\mathcal{A}$  in a field theory to an area of a codimension two minimal surface  $\mathcal{E}_{\mathcal{A}}$ , called the RT surface, in its dual bulk spacetime [15–17]. The entanglement entropy calculated in this way is called the holographic entanglement entropy.

To include the quantum correction, the generalized entropy (fine-grained or von Neumann entropy) in a CFT was proposed in [18]. Soon after, the holographic prescription for the generalized entropy was proposed by including the bulk entropy and finding a quantum extremal surface (QES) [19, 20]. Remarkably, based on the entanglement wedge reconstruction [21], the authors in [22, 23] showed that the Page curve can be obtained in the semiclassical calculation of the generalized entropy by holographic correspondence.

The QES in the context of a two-dimensional Jackiw-Teitelboim (JT) gravity theory coupled to non-gravitational conformal matter, i.e. the so called thermal bath, has been studied in [24, 25]. The bulk entropy was calculated by the double holography scheme. It was found that in order for the Hawking radiation to follow the Page curve for an evaporating black hole, an island should emerge along with a QES inside the horizon at late times to account for unitarity. While for the eternal black hole, it was showed that the QES could be outside the horizon [26–29]. The island formula has soon been extended to higher dimensional spacetime [30–69].

Later on, coupling the JT gravity theory to a thermal bath at a finite temperature has been studied in [70], where the doubly holographic bulk spacetime is a black hole instead of a pure AdS spacetime. However, coupling a higher dimensional gravity theory to a thermal bath at a finite temperature is still not clear.

On the other hand, boundary conformal field theory (BCFT) is a conformal field theory defined

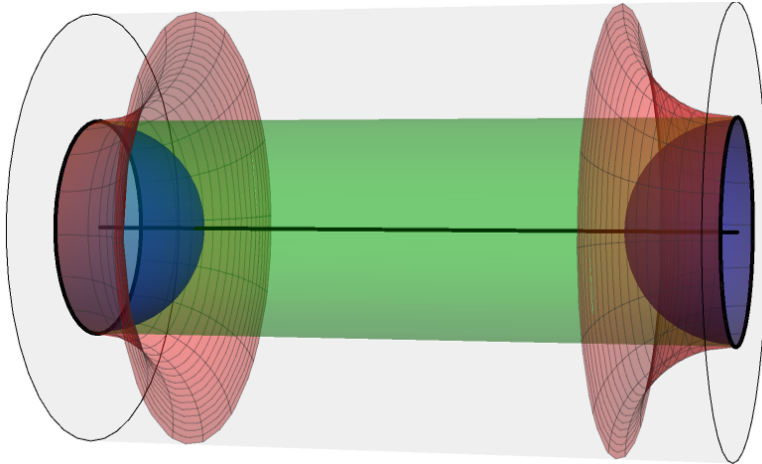


**Figure 1:** The three-dimensional illustration of the BCFT model where the different RT surfaces are displayed. The green inner cylinder is the Hartman-Maldacena surface, the red hat-like surfaces are the boundary RT surfaces, and the blue hemispheres are the island RT surfaces. The boundary/ETW brane of the CFT is represented by the outer cylinder, while the Planck brane is the axis in the middle of the cylinder.

on a manifold with boundaries where suitable boundary conditions are imposed [71]. Early studies of holographic dual of defect or interface CFT can be found in [72, 73]. The holographic dual of BCFT by including extra boundaries in the gravity dual was proposed in [74–76]. In other words, a holographic construction of conformal field theories with boundaries can be established with some appropriate boundary conditions. Using holographic BCFT to study the Page curve has been addressed in [30, 31, 38].

In this paper, we study the holographic entanglement entropy of a  $(d+1)$ -dimensional BCFT at finite temperatures, whose dual bulk spacetime is an asymptotically  $\text{AdS}_{d+2}$  black hole. We introduce a moving end-of-the-world (ETW) brane which is the hypersurface that the earliest Hawking radiation can reach. This ETW brane defines a time-dependent effective radiation region, which supports a new type of RT surface instead of the two known ones, see the sketch in Fig.1. The two black circles on the two ends represent the entanglement surfaces. There are three possible RT surfaces that may appear. One is the two disconnected blue hemispheres that anchors on the entanglement surfaces. Another is the green inner cylinder which connects the entanglement surfaces directly. In addition, there is a third one, the two red hat-like surfaces, if there exists an ETW brane represented by the outer cylinder. This RT surface anchors on both the entanglement surfaces and the ETW brane. We examine the competition among the three RT surfaces that may appear in the course of the evolution of the Page curve by studying the phase transitions among them and the

phase diagram.

This paper is organized as follows. In section 2, we review the basics of holographic entanglement entropy and discuss our setup including the purification, double holography, and BCFT that will be used in our work. In section 3, we calculate the holographic entanglement entropy for the three RT surfaces. In section 4, we examine the phase transitions among the RT surfaces then discuss the phase diagram and the Page curve at different temperatures. We conclude our results in section 5.

## 2 Background and Setup

### 2.1 Generalized Entanglement Entropy

Consider a Hilbert space  $\mathcal{H}$  of a quantum field theory on a Cauchy time slice and divide  $\mathcal{H}$  into two regions  $\mathcal{A}$  and its complement  $\mathcal{A}^c$ . We denote the density matrix of the states in  $\mathcal{H}$  by  $\rho$ . The entanglement entropy between the states in  $\mathcal{A}$  and  $\mathcal{A}^c$  is defined as,

$$\mathcal{S}_{\mathcal{A}} = -\text{Tr} [\rho_{\mathcal{A}} \ln \rho_{\mathcal{A}}], \quad (2.1)$$

where

$$\rho_{\mathcal{A}} = \text{Tr}_{\mathcal{A}^c} \rho, \quad (2.2)$$

is the reduced density matrix of the region  $\mathcal{A}$ .

Assuming the quantum field theory has a dual gravity theory living in a higher dimensional asymptotic AdS bulk spacetime  $\mathcal{M}$  through the holographic correspondence [77, 78], the entanglement entropy between  $\mathcal{A}$  and  $\mathcal{A}^c$  can be calculated by the Ryu-Takayanagi (RT) formula [15, 17],

$$S_{\mathcal{A}}^{\text{class}} = \min_{\mathcal{E}_{\mathcal{A}}} \frac{\text{Area}(\mathcal{E}_{\mathcal{A}})}{4G_N}, \quad (2.3)$$

where  $G_N$  is the Newton constant and  $\mathcal{E}_{\mathcal{A}}$  is a codimension two RT surface in the bulk spacetime  $\mathcal{M}$  which is anchored on the boundary  $\partial\mathcal{A}$  of the entangling region  $\mathcal{A}$ . It is important that the RT surface  $\mathcal{E}_{\mathcal{A}}$  is homologous to  $\mathcal{A}$ . The presence of the boundaries  $\mathcal{Q}$  in the BCFT spacetime allows the RT surface  $\mathcal{E}_{\mathcal{A}}$  to reach the boundary  $\mathcal{Q}$  as shown in Fig.2.

To include the quantum correction, we need to consider the generalized holographic entanglement entropy [18],

$$S_{\mathcal{A}}^{\text{gen}}(\mathcal{E}_{\mathcal{A}}) = \frac{\text{Area}(\mathcal{E}_{\mathcal{A}})}{4G_N} + \mathcal{S}_{\text{bulk}}(\mathcal{E}_{\mathcal{A}}), \quad (2.4)$$

where  $\mathcal{S}_{\text{bulk}}(\mathcal{E}_{\mathcal{A}})$  is the bulk entropy between the entanglement wedge  $\mathcal{R}_{\mathcal{A}}$  bounded by  $\mathcal{A} \cup \mathcal{E}_{\mathcal{A}}$ , and its complementary region in the bulk space.

The fine-grained entanglement entropy is defined as the minimal value of the generalized entanglement entropy,

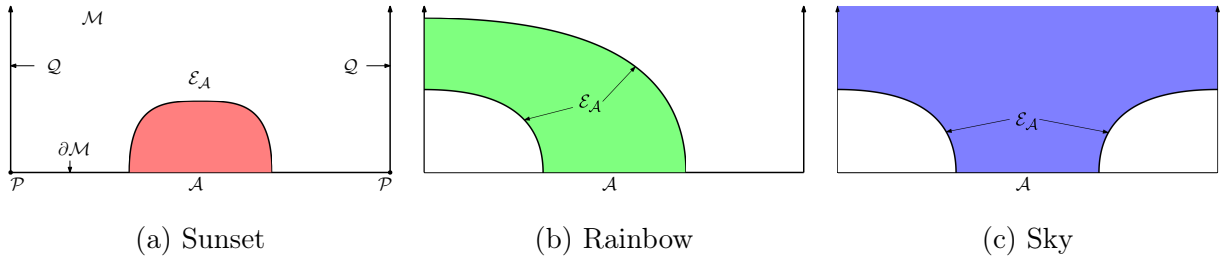


**Figure 2:** Three possible RT surfaces  $\mathcal{E}_A$  of an entangling region  $\mathcal{A}$  extending to the bulk spacetime  $\mathcal{M}$  where the holographic dual gravity theory lives. The colored regions represent the entanglement wedges in different configurations.

$$\mathcal{S}_A = \min_X [S_A^{\text{gen}}(X)] = \min_X \left[ \frac{\text{Area}(X)}{4G_N} + \mathcal{S}_{\text{bulk}}(X) \right], \quad (2.5)$$

where  $X$  is the QES that minimizes the generalized entanglement entropy  $S_A^{\text{gen}}(X)$ .

## 2.2 Black Hole Coupled to Thermal Bath

In the papers of AEM<sup>4</sup>Z [23, 24], a 2d Jackiw-Teitelboim (JT) gravity on  $\text{AdS}_2$  is coupled to a matter  $\text{CFT}_2$ . This 2d system is holographically dual to a 1d quantum mechanical system. If this 2d theory containing a black hole is coupled to a bath which consists of the same  $\text{CFT}_2$  but now living on a flat space, then the black hole is permitted to evaporate into the bath.

To study the Hawking radiation for an evaporating black hole, one has to deal with a time-dependent spacetime. Alternatively, one can consider a thermofield double state (TFD) that is dual to a two-sided eternal black hole [26]. The Penrose diagram of the eternal black hole system is shown in Fig.3. There are two copies of the CFT,  $\text{CFT}_L$  and  $\text{CFT}_R$ , living on the boundaries of two copies of the exterior region (shaded in lighter blue color), which are connected by a wormhole (shaded in darker blue color). The bifurcation dashed lines are the event horizons of the eternal black hole.

The system is time-invariant as time evolves forward on one side while backwards on the other side. However, one can consider time evolving forward on both sides to introduce the time dependence in this system [79].

In addition, in order to allow the eternal black hole to radiate, we couple two copies of an auxiliary thermal bath (shaded in light yellow color) at the boundaries of the two exterior regions. The two copies of the thermal bath are in flat spacetime and have the same finite temperature  $T$  with the black hole. The eternal black hole together with the two copies of the thermal bath comprises a pure system.

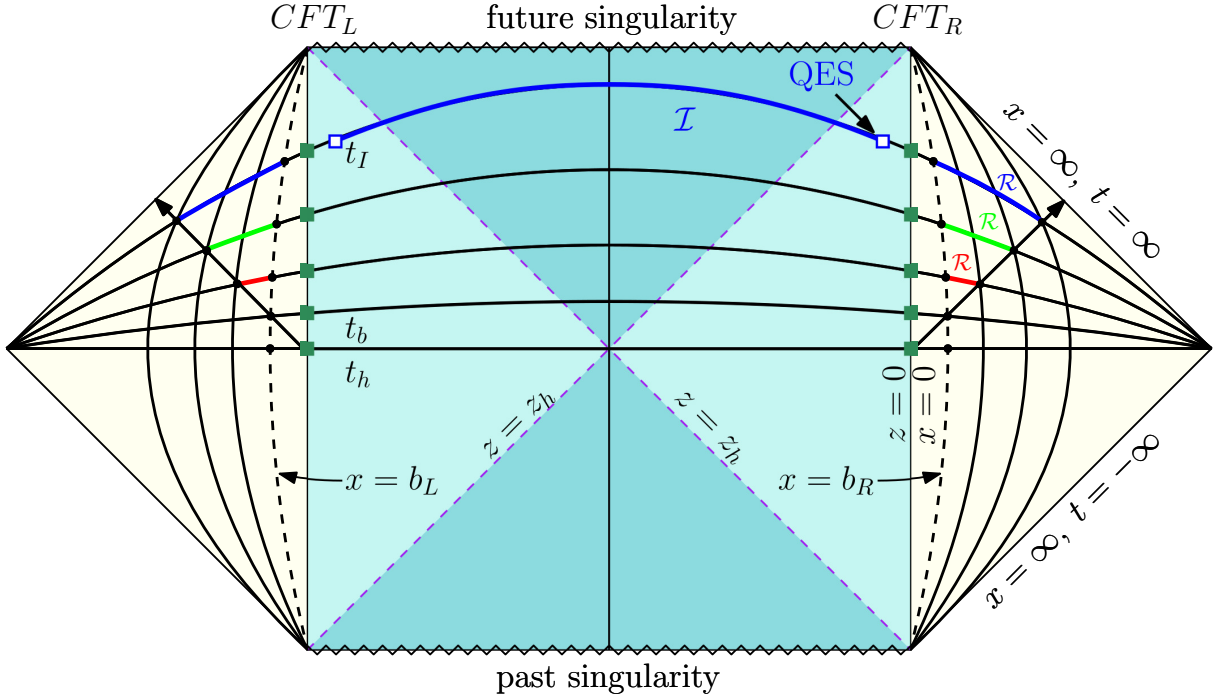


**Figure 3:** The Penrose diagram of the two-sided eternal black hole. The violet dashed lines represent the event horizon of the black hole ( $z = z_h$ ), which separates the black hole into interior (darker blue) and exterior (lighter blue) regions. Two copies of the CFT live on the two boundaries of the eternal black hole. Two copies of the bath (light yellow) are coupled to the boundaries of the black hole. The vertical dashed curves are the cutoff at  $x = b_{L,R}$ . The vertical solid curves represent the ETW brane at different times. The horizontal curves are Cauchy slices at different boundary times with the red, green, and blue fragments representing the entanglement regions of the Hawking radiation. The 45 degree lines with arrows are the outgoing null surfaces on which the Hawking radiation travels.

We are going to calculate the entanglement entropy of the CFTs on the boundaries of the exterior regions using the generalized entanglement entropy in eq.(2.5). To do so, we introduce a cutoff at  $x = b_{L,R}$  which is slightly inside the bath region. The cutoff separates the whole system into two regions: the gravitational region that includes the black hole with its boundaries, and the radiation region where the Hawking radiation escapes. The entanglement region is thus the surface at the cutoff  $x = b_{L,R}$ .

Through the holographic correspondence, the entanglement entropy of the CFTs can be obtained by finding a minimal area surface in the bulk gravity spacetime that is homologous to the entanglement region. Classically, the minimal surface is the union of the two horizons, i.e. the

classical RT surface, which is a time independent constant. The classical RT surface gives the coarse-grained entropy that sets the upper bound of the entanglement entropy of the Hawking radiation.

Including quantum corrections, the QES is the surface that minimizes the generalized entanglement entropy eq.(2.5). The location of the QES on a Cauchy slice is generically different at different slices, so the fine-grained entropy of the eternal black hole is time-dependent. Furthermore, there could be more than one QES that minimize the entanglement entropy locally. The dominant QES should be the one which globally minimizes the entanglement entropy. This implies the possible phase transitions between different QES.

Having the basic picture in mind, let us now consider the radiation region in more detail. We couple the bath to the eternal black hole at a certain time  $t = t_h$ . We assign the bath to have the same temperature as that in the eternal black hole. As the Hawking radiation from the black hole escapes to the thermal bath, there is the same amount of energy that goes back to the black hole from the bath so that the whole system is in thermodynamic equilibrium.

To decode the information inside the black hole, we need to measure the Hawking radiation escaping to the thermal bath. Once the Hawking radiation has entered the bath, it then travels along the outgoing null surface with the speed of light as shown in Fig.3. At time  $t = t_b$ , the earliest Hawking radiation reaches the cutoff and enters into the radiation region. We then start to measure the Hawking radiation from the time  $t_b$  and set it as our initial time.

At a later time  $t > t_b$ , the earliest radiation will reach a surface of distance  $L = b + c(t - t_b)$  which behaves as an end-of-the-world (ETW) brane. Since there is no radiation beyond the ETW brane, the effective radiation region is just the space-like region between the cutoff and the ETW brane, namely  $[b_L, L] \cup [b_R, L]$ , which increases with time. The ETW brane at different times are plotted as vertical curves in Fig.3.

As we have mentioned, the whole system including both the eternal black hole and the thermal bath is a pure system, so that the bulk entanglement entropy in eq.(2.5) equals the entanglement entropy of the Hawking radiation in the effective radiation region  $\mathcal{R}$  as shown in the Fig.3. The entanglement entropy of the radiation region  $\mathcal{R}$  can be calculated using the island formula [24, 35],

$$\mathcal{S}_{EE}(\mathcal{R}) = \min \left\{ \text{ext} \left( S(\mathcal{R} \cup \mathcal{I}) + \frac{\text{Area}(\partial \mathcal{I})}{4G_N^{(d+1)}} \right) \right\}, \quad (2.6)$$

It can be shown that, at early times, the entanglement entropy of the effective radiation region is always dominated by the vanishing island  $\mathcal{I} = \emptyset$  with  $\text{Area}(\partial \mathcal{I}) = 0$ . The bulk entropy  $S(\mathcal{R} \cup \emptyset)$  corresponding to the vanishing island, monotonically increases from zero and will eventually exceed the coarse grained entropy implying the information paradox.

Remarkably, there exists a non-trivial QES outside of the horizon for the eternal black hole [79] that implies a non-vanishing island  $\mathcal{I}$  between the two non-trivial QES. The bulk entropy corresponding to this non-vanishing island equals to the entanglement entropy of the union of the radiation region with the island and will dominate at late times as shown in the Fig.3.

Since the QES is outside of the horizon, the generalized entanglement entropy for the non-vanishing island is a constant. At a later time, e.g.  $t = t_I$  in Fig.3, the non-vanishing island case will dominate the system. The time at which the phase transition between the vanishing and non-vanishing island takes place is called the Page time. The phase transition of the generalized entanglement entropy leads to the well known Page curve for the eternal black hole.

The eternal black hole in 2-dimensions has been studied in [26]. Extension to higher dimensions was previously considered in [35]. The main difficulty in obtaining the generalized entanglement entropy is calculating the bulk entropy in curved spacetime. In 2-dimensions, the replica trick is used to compute the entanglement entropy through the path integral approach. However, this trick is difficult to be generalized to higher dimensions.

In section 2.3, we will use the idea of the double holography to calculate the bulk entanglement entropy [24]. It has been shown that combining double holography with BCFT is a powerful method to calculate the bulk entanglement entropy and can be generalized to higher dimensions [41].

### 2.3 Double Holography

To calculate the bulk entanglement entropy in JT gravity, the authors of [24, 25] introduced a 3d spacetime that is holographically dual to the 2d matter CFTs and the baths, i.e. the double holographic duality. The 3d double holographic bulk metric is locally an  $\text{AdS}_3$  spacetime with a boundary on which the 2d theory is living. This is similar to the Randall-Sundrum model, where the boundary is called the Planck brane [72, 80, 81].

Extending this idea to a higher dimensional thermofield double state as discussed in [35], there are three perspectives to describe the system. In the *boundary perspective*, a pair of  $(d + 1)$ -dimensional CFTs live on a region  $[0, L]$  with a  $d$ -dimension CFT living on its boundary at  $x = 0$  indicated by the green square dots as shown in Fig.4(a). where  $x = b_{L,R}$  is the cutoff and the other boundary is at  $x = L$ . The effective Hawking radiation region is  $[b_L, L] \cup [b_R, L]$ .

The *brane perspective* can be realized by using holographic correspondence to replace the  $\text{CFT}_d$  by a Planck brane on which an asymptotically  $\text{AdS}_{d+1}$  eternal black hole lives, as shown in Fig.4(b). We assign the radial direction of the eternal black hole as  $z$  with the  $\text{CFT}_d$  sitting at  $z = 0$ . The horizons of the eternal black hole are indicated by the two purple square dots. As argued in [34, 72, 82–88], the transparent boundary condition between the gravitational and the radiation regions imply that the stress tensor in  $\text{CFT}_d$  is not conserved and will generate an anomalous

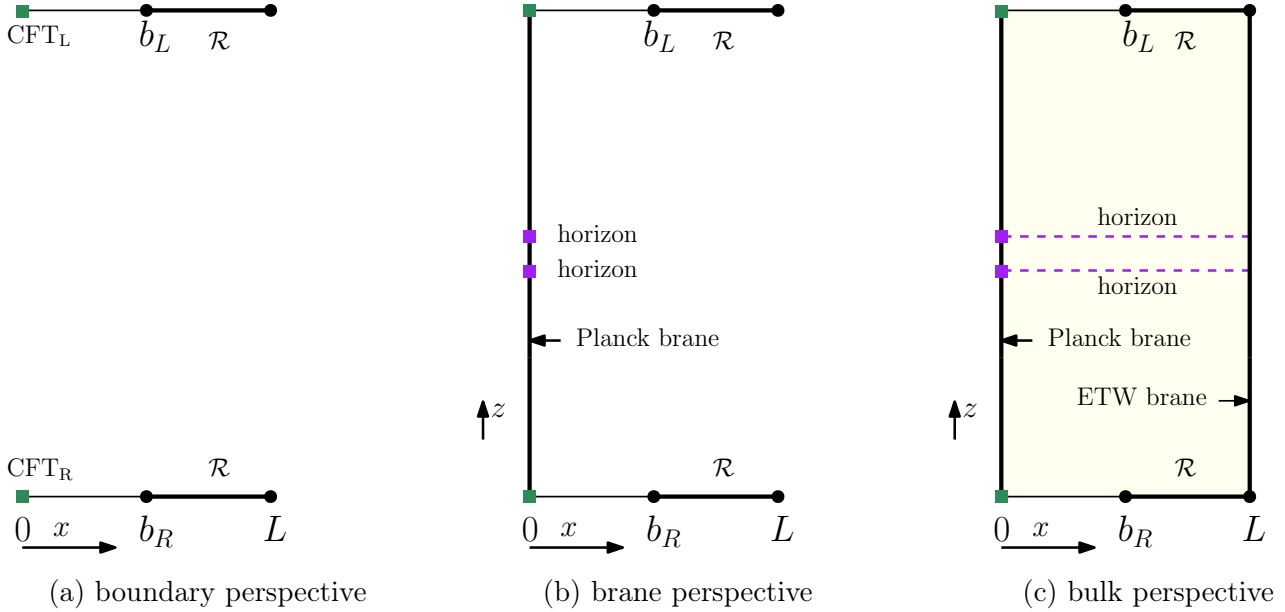


**Figure 4:** Three different perspectives of the gravity system, Hawking radiation system and the holographic dual of these systems.

dimension, so that the dual graviton gets a mass. However, if the central charge of the  $CFT_d$  is large, the effect from the mass can be negligible.

In the *bulk perspective*, we use the holographic correspondence again to replace the  $CFT_{d+1}$  by an asymptotically  $AdS_{d+2}$  black hole bulk spacetime. This geometry can be properly described by a holographic BCFT setup, as shown in Fig.4(c). The  $(d+1)$ -dimensional BCFT is dual to an  $AdS_{d+2}$  black hole bulk spacetime. The boundary  $x = 0$  extends to the bulk spacetime as a Planck brane and the other boundary  $x = L$  extends to the bulk spacetime as an ETW brane. The embedding of the branes into the bulk spacetime is determined by solving the holographic BCFT system. The purple dashed lines represent the two horizons in the bulk black hole. In the bulk perspective, the bulk entanglement entropy in eq.(2.4) can be calculated by a *classical* RT surface in the bulk spacetime anchored on the entangling surface at  $x = b_{L,R}$ .

In summary, in our setup, the boundary on the left corresponds to the gravitational region containing the Planck brane and a small region to the left of the cutoff at  $x = b_{L,R}$ . The other boundary on the right at  $x = L$  corresponds to an ETW brane which moves at the speed of light to the right. The effective radiation region is  $[b_L, L] \cup [b_R, L]$ .

## 2.4 Brief Review of Black Hole Solution in BCFT

In this subsection, we will briefly review a black hole solution in the holographic BCFT that we will use in this work.

The  $(d+2)$ -dimensional bulk spacetime  $\mathcal{M}$  is holographically dual to a  $(d+1)$ -dimensional CFT defined on the conformal boundary  $\partial\mathcal{M}$ .  $\partial\mathcal{M}$  has a  $d$ -dimensional boundary  $\mathcal{P}$ , which has a  $(d+1)$ -dimensional hypersurface dual  $\mathcal{Q}$  in  $\mathcal{M}$  anchored at  $\mathcal{P}$ , see Fig.2.

The action of the gravitational theory in the bulk is,

$$S = S_{\mathcal{M}} + S_{GHY} + S_{\mathcal{Q}} + S_{\partial\mathcal{M}} + S_{\mathcal{P}}, \quad (2.7)$$

where

$$S_{\mathcal{M}} = \int_{\mathcal{M}} \sqrt{-g}(R - 2\Lambda_{\mathcal{M}}), \quad (2.8)$$

$$S_{\mathcal{Q}} = \int_{\mathcal{Q}} \sqrt{-h}(R_{\mathcal{Q}} - 2\Lambda_{\mathcal{Q}} + 2K), \quad (2.9)$$

$$S_{\partial\mathcal{M}} = 2 \int_{\partial\mathcal{M}} \sqrt{-\gamma}K', \quad (2.10)$$

$$S_{\mathcal{P}} = 2 \int_{\mathcal{P}} \sqrt{-\sigma}\theta. \quad (2.11)$$

$S_{\mathcal{M}}$  is the Einstein–Hilbert action of  $\mathcal{M}$  with  $R$  and  $\Lambda_{\mathcal{M}}$  being the intrinsic Ricci curvature and the cosmological constant of  $\mathcal{M}$  respectively.  $S_{GHY}$  is the Gibbons–Hawking–York boundary term.  $S_{\mathcal{Q}}$  is the action of the  $(d+1)$ -dimensional hypersurface  $\mathcal{Q}$  with the induced metric  $h_{ab} = g_{ab} - n_a^{\mathcal{Q}}n_b^{\mathcal{Q}}$ , where  $n^{\mathcal{Q}}$  is the unit normal vector of  $\mathcal{Q}$ , and  $R_{\mathcal{Q}}$ ,  $\Lambda_{\mathcal{Q}}$ ,  $K$  being the intrinsic Ricci curvature, the cosmological constant and the extrinsic curvatures of  $\mathcal{Q}$  in  $\mathcal{M}$  respectively.  $S_{\partial\mathcal{M}}$  is the action of the conformal boundary  $\partial\mathcal{M}$  with the induced metric  $\gamma_{ab} = g_{ab} - n_a^{\partial\mathcal{M}}n_b^{\partial\mathcal{M}}$ , where  $n^{\partial\mathcal{M}}$  is the unit normal vector of  $\partial\mathcal{M}$ , and  $K'$  is the extrinsic curvature of  $\partial\mathcal{M}$ .  $S_{\mathcal{P}}$  is the boundary term of  $\mathcal{Q}$  and  $\partial\mathcal{M}$  with  $\sigma_{ab}$  being the metric of  $\mathcal{P}$  and  $\theta = \cos^{-1}(n^{\mathcal{Q}} \cdot n^{\partial\mathcal{M}})$  being the supplementary angle between  $\mathcal{Q}$  and  $\partial\mathcal{M}$ , which makes a well-defined variational principle on  $\mathcal{P}$ .

Comparing the above BCFT system with the Penrose diagram in Fig.3,  $\mathcal{Q}$  represents the Planck brane containing the eternal black hole (blue region),  $\partial\mathcal{M}$  represents the thermal baths (light yellow region), and  $\mathcal{P}$  is the boundary of the eternal black hole at  $x = 0$  where the CFTs live.

A simple asymptotic AdS black hole solution of the above system has been obtained in [89],

$$ds_{\mathcal{M}}^2 = \frac{l_{AdS}^2}{z^2} \left[ -f(z)dt^2 + \frac{dz^2}{f(z)} + dx^2 + \sum_{i=1}^{d-1} (dx_i)^2 \right], \quad (2.12)$$

where

$$f(z) = 1 - \frac{z^{d+1}}{z_h^{d+1}}, \quad (2.13)$$

and  $z_h$  corresponds to the horizon of the black hole. The  $(d+1)$ -dimensional conformal boundary  $\partial\mathcal{M}$  is at  $z = 0$ . The temperature of the BCFT is given by the Bekenstein-Hawking temperature of the black hole,

$$T = \frac{d+1}{4\pi z_h}. \quad (2.14)$$

In the double holographic setup, there are two  $(d+1)$ -dimensional hypersurfaces  $\mathcal{Q}$ s, the Planck brane and the ETW brane. By varying  $S_{\mathcal{Q}}$  with  $h^{ab}$  we get the equations of motion of  $\mathcal{Q}$ ,

$$R_{\mathcal{Q}ab} + 2K_{ab} - \left( \frac{1}{2}R_{\mathcal{Q}} + K - \Lambda_{\mathcal{Q}} \right) h_{ab} = 0, \quad (2.15)$$

which is the Neumann boundary condition proposed by Takayanagi in [74]. This condition is too strong and gives more constraint equations than the degrees of freedom, so in [90, 91], the following mixed boundary condition is proposed by Chu et al.

$$(d-1)(R_{\mathcal{Q}} + 2K) - 2(d+1)\Lambda_{\mathcal{Q}} = 0. \quad (2.16)$$

The induced metric  $h_{ab}$  of the Planck brane and the ETW brane is,

$$ds_{\mathcal{Q}} = \frac{l_{AdS}^2}{z^2} \left[ -f(z)dt^2 + \frac{dz^2}{f(z)} + \sum_{i=1}^{d-1} (dx_i)^2 \right], \quad (2.17)$$

with a simple embedding  $x = \text{constant}$ . The intrinsic curvature, extrinsic curvature, and the cosmological constant on  $\mathcal{Q}$  are,

$$R_{\mathcal{Q}} = -\frac{d(d+1)}{l_{AdS}^2}, \quad K_{ab} = 0, \quad \Lambda_{\mathcal{Q}} = -\frac{d(d-1)}{2l_{AdS}^2}, \quad (2.18)$$

which satisfies the mixed boundary condition eq.(2.16). In all of the calculations, we are going to denote the  $(d-1)$ -dimensional volume as,

$$\int d^{d-1}\mathbf{x} = V_{d-1}. \quad (2.19)$$

### 3 Holographic Entanglement Entropy of Hawking Radiation

As we have explained in section 2.3, we are going to calculate the entanglement entropy with the effective radiation region  $[b_L, L] \cup [b_R, L]$  as the entanglement region. By holographic correspondence,

it is proportional to the area of the RT surface in the doubly holographic bulk spacetime. The RT surface is anchored at the entanglement surface  $x = b_{L,R}$  and is homologous to the effective radiation region  $[b_L, L] \cup [b_R, L]$ . At the leading order, we only need to consider the classical RT surface,

$$S = \int d^{d+1}\xi \mathcal{L} = \int d^{d+1}\xi \sqrt{\det G_{ab}}, \quad (3.1)$$

where the induced metric is defined by

$$G_{ab} = g_{\mu\nu} \partial_a X^\mu \partial_b X^\nu, \quad (3.2)$$

and the bulk metric  $g_{\mu\nu}$  is given in eq.(2.12).

Generically, there could be more than one QES with each of them being a locally minimum surface. In the following of this section, we will find that there are three RT surfaces in our system. One is the *Hartman-Maldacena surface* (HM), which penetrates the horizon and connects the cutoff at  $x = b_{L,R}$ . Another one is the *boundary RT surface* (BRT), which is anchored not only on the cutoffs at  $x = b_{L,R}$  but also on the ETW brane at  $x = L$ . The third one is the *island RT surface* (IRT) that starts from the cutoff  $x = b_{L,R}$  and is anchored on the Planck brane at the quantum extremal surfaces at  $z = z_{\text{QES}}$ . The region between the QES and its symmetric copy is the island which includes the whole interior of the eternal black hole.

The RT surfaces at different times are shown in Fig.5. The red/green/blue line represents the BRT/HM/IRT surface. At time  $t = t_h$ , as shown in Fig.5(a), the Hawking radiation from the black hole reaches the boundary  $z = 0$  and enters into the thermal bath at  $x = 0$ . At the initial time  $t = t_b$ , as shown in Fig.5(b), the Hawking radiation reaches the cutoff  $x = b$  and enters into the effective radiation region. Since the ETW brane is located at  $x = b_R$  at the initial time  $t = t_b$ , the BRT surface shrinks to zero, and only the HM and the IRT surfaces are present as shown in Fig.5(b).

The BRT surface dominates the system at the early time with the red region being the entanglement wedge as shown in Fig.5(c). As time evolves, the stretching of the interior of the black hole causes the growth of the HM surface. However, at the same time, the ETW brane moves to the right with the speed of light  $c$  and coordinate  $L = b + c(t - t_b)$ , so that the BRT surface increases faster than the HM surface. At a certain time, the BRT surface will exceed the HM surface and the latter becomes dominant with the green region being the entanglement wedge as shown in Fig.5(d).

Finally, after a critical time, the BRT and HM surfaces will exceed the IRT surface so that it becomes dominant with the blue region being the entanglement wedge as shown in Fig.5(e). When the IRT surface dominates, the entanglement wedge includes the part between the QESs on the Planck brane, i.e. the island. Since the QES is outside of the horizon in the eternal black hole, the island contains the whole interior of the black hole. Based on the entanglement wedge

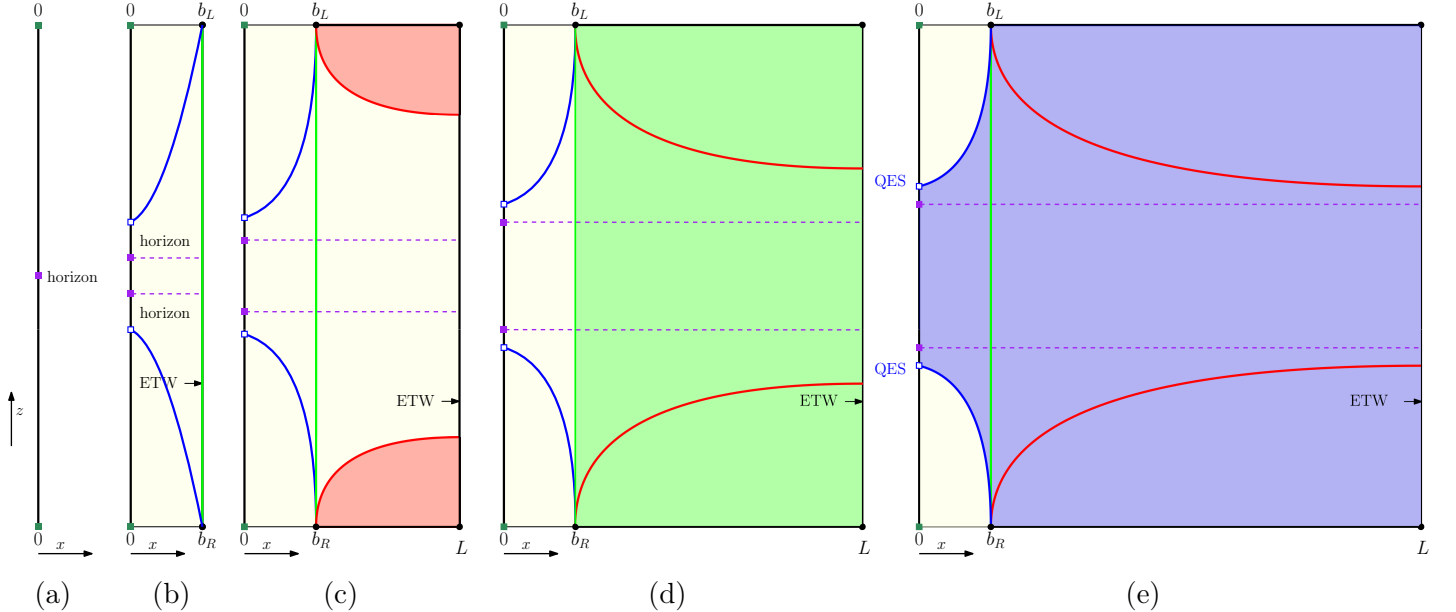


**Figure 5:** The time evolution of the RT surfaces in the BCFT system. The red/green/blue line represents the BRT/HM/IRT surface. The color of the shaded region represents the entanglement wedge whose entanglement entropy is dominant at that time.

reconstruction, after the critical time, we are able to reconstruct all the information inside the black hole from the data observed in the effective radiation region. The critical time is called the Page time  $t_P$ .

### 3.1 Hartman-Maldacena Surface

Since the bulk spacetime is symmetric, we calculate only one side. However, the complete description of the entanglement entropy can be considered by taking into account the two sides. The HM surface is a locally minimum surface penetrating the horizon and connecting the two cutoffs at  $x = b_{L,R}$ . To describe the interior region behind the horizon, we make the following coordinate transformation,

$$t = v + \int \frac{dz}{f(z)} \Rightarrow dt = dv + \frac{dz}{f(z)}. \quad (3.3)$$

The metric eq.(2.12) then becomes,

$$ds^2 = \frac{l_{AdS}^2}{z^2} \left[ -f(z)dv^2 - 2dvdz + dx^2 + \sum_{i=1}^{d-1} dx_i^2 \right], \quad (3.4)$$

where the HM surface is described by  $x = b_R$  and  $v = v(z)$ .

The entanglement entropy eq.(3.1) on the  $t - z$  plane (or the  $v - z$  plane) after the coordinate transformation eq.(3.3), can be calculated as,

$$\mathcal{S}_{\text{HM}} = \frac{l_{AdS}^d}{4G_N^{(d+2)}} \int dz d^{d-1}x \frac{1}{z^d} \sqrt{- \left( \frac{dv}{dz} \right) \left( f(z) \left( \frac{dv}{dz} \right) + 2 \right)}. \quad (3.5)$$

The conjugate momentum of  $v$  is,

$$\frac{\partial \mathcal{L}}{\partial v'} = C_v = \frac{f(z)v' + 1}{z^d \sqrt{-v'(f(z)v' + 2)}}, \quad (3.6)$$

where  $v' = dv/dz$ . From eq.(3.6) we can solve for  $v'$  as,

$$v' = \frac{1}{f(z)} \left[ -1 \pm \sqrt{\frac{C_v^2 z^{2d}}{f(z) + C_v^2 z^{2d}}} \right]. \quad (3.7)$$

We choose the solution with the negative square root and integrate it on  $z$  to get,

$$v = \int_0^{z_M} \frac{dz}{f(z)} \left[ -1 - \sqrt{\frac{C_v^2 z^{2d}}{f(z) + C_v^2 z^{2d}}} \right], \quad (3.8)$$

where  $z_M$  is the turning point of the HM surface with the boundary time  $t$  as shown in Fig.6. Substituting eq.(3.8) back into eq.(3.3), we obtain the expression of the boundary time,

$$t = - \int_0^{z_M} \frac{C_v z^d dz}{f(z) \sqrt{f(z) + C_v^2 z^{2d}}}. \quad (3.9)$$

The turning point of the HM surface can be found by imposing a boundary condition at  $z = z_M$ ,

$$\left. \frac{dz}{dv} \right|_{z=z_M} = f(z_M) \sqrt{\frac{f(z_M) + C_v^2 z_M^{2d}}{-f(z_M)}} = 0, \quad (3.10)$$

which leads to the following expression of the conjugate momentum  $C_v$  in terms of  $z_M$ ,

$$C_v^2 = - \frac{f(z_M)}{z_M^{2d}}. \quad (3.11)$$

As we have mentioned above, we will use

$$t_h = - \int_0^{z_h} \frac{\sqrt{f(z_h)} z^d dz}{f(z) \sqrt{f(z_h) z^{2d} - f(z) z_h^{2d}}}, \quad (3.12)$$

as the reference time as shown in Fig.6.

Plugging eq.(3.7) and eq.(3.11) into eq.(3.5), we finally obtain the entanglement entropy corresponding to the HM surface,

$$\mathcal{S}_{\text{HM}} = \frac{l_{AdS}^d \cdot V_{d-1}}{4G_N^{(d+2)}} \int_0^{z_M} \frac{z_M^d dz}{z^d \sqrt{f(z) z_M^{2d} - f(z_M) z^{2d}}}. \quad (3.13)$$

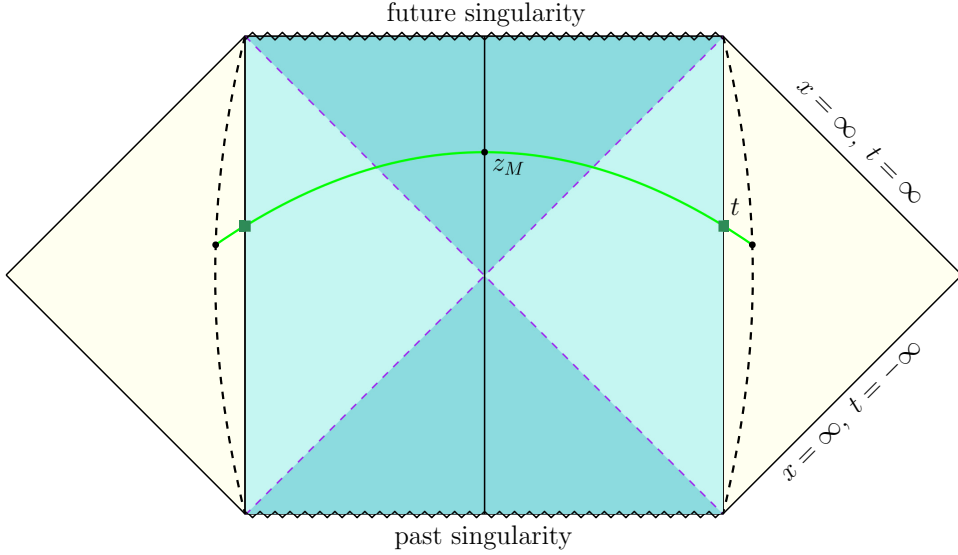


**Figure 6:** The Hartman-Maldacena Surface at time  $t$ .

### 3.2 Boundary RT Surface

The effective Hawking radiation region at a fixed time is<sup>1</sup>

$$\mathcal{R} = \{x \in \mathbb{R}, \mathbf{x}_{d-1} \in \mathbb{R}^{d-1} \mid x \in (b_R, L), x_i \in \mathbb{R} \quad \text{for } i = 1, 2, \dots, d-1\}, \quad (3.14)$$

which preserves  $(d-1)$ -dimensional translation invariance, so that we can describe the BRT surface by  $t = \text{constant}$  and  $z = z(x)$ . The entanglement entropy eq.(3.1) on the  $z - x$  plane can be calculated as,

$$\mathcal{S}_{\text{BRT}} = \frac{\ell_{AdS}^d}{4G_N^{(d+2)}} \int dx d^{d-1} \mathbf{x} \frac{1}{z^d} \sqrt{1 + \frac{1}{f(z)} \cdot \left(\frac{dz}{dx}\right)^2}. \quad (3.15)$$

The conjugate momentum of  $z(x)$  is,

$$p_z = \frac{\partial \mathcal{L}}{\partial z'} = \frac{z'}{z^d \cdot f(z) \sqrt{1 + \frac{z'^2}{f(z)}}}, \quad (3.16)$$

where  $z' = dz/dx$ . The Hamiltonian can be calculated as,

$$\mathcal{H} = z' p_z - \mathcal{L} = \frac{-1}{z^d \sqrt{1 + \frac{z'^2}{f(z)}}}. \quad (3.17)$$

---

<sup>1</sup>Due to the symmetry between the left and right sides, we will only consider the right side as the example in the following calculations. The calculation for the left side is exactly the same.

Since the Lagrangian  $\mathcal{L}$  is not explicitly dependent on  $x$ , the Hamiltonian is conserved. We thus define a constant,

$$C_z = \frac{-1}{z^d \sqrt{1 + \frac{z'^2}{f(z)}}}. \quad (3.18)$$

From eq.(3.18), we can solve for  $z'$  as,

$$z' = \pm \frac{\sqrt{f(z) \left( \frac{1}{C_z^2} - z^{2d} \right)}}{z^d}. \quad (3.19)$$

It has been shown that the minimum surface must be perpendicular to the ETW brane [91], so that we have the following boundary conditions,

$$z(x = b_R) = 0, \quad \left. \frac{dz}{dx} \right|_{x=L} = 0. \quad (3.20)$$

Applying eq.(3.18) at  $x = L$ , we can determine the constant,

$$C_z = -\frac{1}{z_L}, \quad (3.21)$$

where  $z_L = z(L)$  is the location that the BRT surface reaches on the ETW brane at  $x = x_L$ . By integrating eq.(3.19) and using eq.(3.21), the length of the effective radiation region can be calculated,

$$L - b_R = \int_0^{z_L} \frac{z^d dz}{\sqrt{f(z)(z_L^{2d} - z^{2d})}}. \quad (3.22)$$

Plugging eq.(3.19) and eq.(3.21) into eq.(3.15), we finally obtain the entanglement entropy corresponding to the BRT surface,

$$\mathcal{S}_{\text{BRT}} = \frac{l_{AdS}^d \cdot V_{d-1}}{4G_N^{(d+2)}} \int_0^{z_L} \frac{z_L^d dz}{z^d \sqrt{f(z)(z_L^{2d} - z^{2d})}}. \quad (3.23)$$

The entanglement entropy defined in eq.(3.23) is divergent near  $z = 0$ . For the purpose of our numerical calculations, we regularize it as,

$$\mathcal{S}_{\text{BRT-reg}} = \frac{l_{AdS}^d \cdot V_{d-1}}{4G_N^{(d+2)}} \left[ \int_0^{z_L} \frac{z_L^d dz}{z^d \sqrt{f(z)(z_L^{2d} - z^{2d})}} - \int_0^{z_L} \frac{z_L^d dz}{z^d \sqrt{(z_L^{2d} - z^{2d})}} \right]. \quad (3.24)$$

We note that the entanglement entropies corresponding to the HM surface, which we calculated in the last subsection, and the IRT surface, which we will calculate in the next subsection, have the same divergence. However, since we are only concerned about the difference between the entanglement entropies, the divergences will cancel each other out, so that we do not need to regularize the other ones. The regularization of the BRT in eq.(3.24) is only for the purpose of numerical plotting.

### 3.3 Island RT Surface

The entanglement entropy of the IRT surface on the  $z - x$  plane reads,

$$\mathcal{S}_{\text{IRT}} = \frac{l_{AdS}^d}{4G_N^{(d+2)}} \left[ \int dx d^{d-1} \mathbf{x} \frac{1}{z^d} \sqrt{1 + \frac{1}{f(z)} \cdot \left( \frac{dz}{dx} \right)^2} + \frac{1}{z_I^{d-1}} \right], \quad (3.25)$$

which is the same as  $\mathcal{S}_{\text{BRT}}$  in eq.(3.15) with an extra term representing the contribution from the QES. Also,  $z_{\text{QES}} = z_I$  is the location of the QES on the Planck brane as shown in Fig.3. In a similar way to section 3.2, we can define a constant  $C_\sigma$ ,

$$C_\sigma = \frac{-1}{z^d \sqrt{1 + \frac{z'^2}{f(z)}}}, \quad (3.26)$$

and solve for  $z'$  as,

$$z' = \pm \frac{\sqrt{f(z) \left( \frac{1}{C_\sigma^2} - z^{2d} \right)}}{z^d}. \quad (3.27)$$

However, in the presence of the QES, the IRT surface does not need to be perpendicular to the Planck brane. The boundary conditions now are given by,

$$z(x=0) = z_I, \quad z(x=b_R) = 0, \quad (3.28)$$

With the above boundary conditions, we get,

$$\frac{dz}{dx} = \pm \frac{\sqrt{f(z) \left( z_I^{2d} - z^{2d} + \frac{z_I^{2d} \sigma^2}{f(z_I)} \right)}}{z^d}, \quad (3.29)$$

which can be integrated to give,

$$b_R = \int_0^{z_I} \frac{z^d dz}{\sqrt{f(z) \left( z_I^{2d} - z^{2d} + \frac{z_I^{2d} \sigma^2}{f(z_I)} \right)}}, \quad (3.30)$$

where  $\sigma = dz/dx|_{x=0}$  is the slope as the IRT surface reaches the Planck brane at  $x = 0$ . The slope  $\sigma$  can be determined by finding the location  $z_I$  of the QES on the Planck brane that minimizes  $\mathcal{S}_{\text{IRT}}$  for a fixed cutoff  $b_R$ . Without the QES contribution, the minimum condition implies  $\sigma = 0$ , i.e. the RT surface is perpendicular to the brane as we have known.

Finally, the entanglement entropy corresponding to the IRT surface eq.(3.25) can be expressed as,

$$\mathcal{S}_{\text{IRT}} = \frac{l_{AdS}^d \cdot V_{d-1}}{4G_N^{(d+2)}} \left[ \int_0^{z_I} \frac{z_I^d}{z^d} \sqrt{\frac{\left( 1 + \frac{\sigma^2}{f(z_I)} \right)}{f(z) \left( z_I^{2d} - z^{2d} + \frac{z_I^{2d} \sigma^2}{f(z_I)} \right)}} dz + \frac{1}{z_I^{d-1}} \right]. \quad (3.31)$$

Now, the condition for the location  $z_I$  of the QES on the Planck brane that minimize  $\mathcal{S}_{\text{IRT}}$  is,

$$\frac{d\mathcal{S}_{\text{IRT}}}{dz_I} = 0. \quad (3.32)$$

Combining eq.(3.30) and eq.(3.32), we can solve for  $z_I$  as well as  $\sigma$  for a fixed  $b_R$ .

## 4 Phase Transitions and Page Curve

As we have seen in the last section, there are three RT surfaces in the eternal black hole system, i.e. the HM, BRT, and IRT surfaces, whose corresponding entanglement entropies have been calculated in eq.(3.13), eq.(3.23), and eq.(3.31). The dominant one is the minimum among them,

$$\mathcal{S} = \min(\mathcal{S}_{\text{HM}}, \mathcal{S}_{\text{BRT}}, \mathcal{S}_{\text{IRT}}). \quad (4.1)$$

Among the three entanglement entropies,  $\mathcal{S}_{\text{IRT}}$  is a constant at a fixed temperature, while the other two increase with time. At the initial time  $t = t_b$ ,  $\mathcal{S}_{\text{BRT}} = 0$  dominates. At a later time, there could be phase transitions between each pair of the three entanglement entropies. In this section, we will investigate the phase transitions in detail and obtain the Page curve for the entanglement entropy of the eternal black hole.

### 4.1 Phase Transitions

To be concrete in this subsection, we set the cutoff  $b_L = b_R = b = 0.1$ , and the black hole horizon  $z_h = 10$  which corresponds to the temperature  $T = 0.032$ .

Since the entanglement entropy corresponding to the IRT surface is a time independent constant, we will first consider the phase transitions between the IRT surface and the other two surfaces. The phase transition between  $\mathcal{S}_{\text{BRT}}$  and  $\mathcal{S}_{\text{IRT}}$  can be obtained from

$$\Delta\mathcal{S}_{\text{BRT-IRT}} = \mathcal{S}_{\text{BRT}} - \mathcal{S}_{\text{IRT}} = 0, \quad (4.2)$$

where  $\mathcal{S}_{\text{BRT}}$  and  $\mathcal{S}_{\text{IRT}}$  are given in eq.(3.23) and eq.(3.31).

The regularized<sup>2</sup> entanglement entropy corresponding to the BRT and IRT surfaces are plotted in Fig.7(a).  $\mathcal{S}_{\text{BRT}}$  (red line) starts from zero at  $t = t_b$  and increases almost linearly. It dominates until  $t - t_b = t_{\text{BRT-IRT}} \simeq 12.01$  when the phase transition between  $\mathcal{S}_{\text{BRT}}$  and  $\mathcal{S}_{\text{IRT}}$  (blue line) takes place, then  $\mathcal{S}_{\text{IRT}}$  will dominate for  $t - t_b > t_{\text{BRT-IRT}}$ .

Similarly, the phase transition between  $\mathcal{S}_{\text{HM}}$  and  $\mathcal{S}_{\text{IRT}}$  can be obtained from

---

<sup>2</sup>We regularize the entanglement entropy using eq.(3.24) to plot it numerically. However, we should note that the exact phase transition time is determined from eq.(4.2) without regularization.

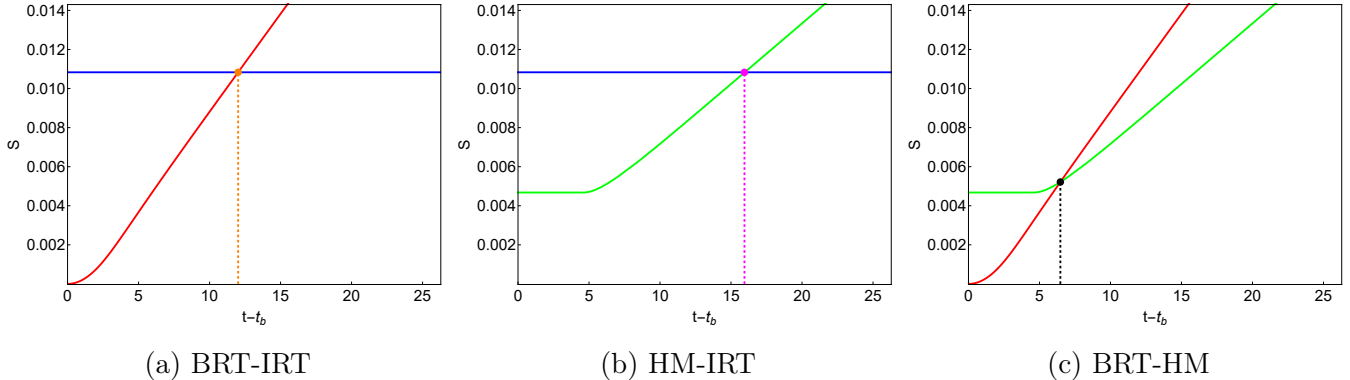


**Figure 7:** The phase transitions between BRT (red), HM (green), and IRT (blue) surfaces for  $z_h = 10$ . (a)  $\mathcal{S}_{\text{BRT}}$  and  $\mathcal{S}_{\text{IRT}}$ . (b)  $\mathcal{S}_{\text{HM}}$  and  $\mathcal{S}_{\text{IRT}}$ . (c)  $\mathcal{S}_{\text{BRT}}$  and  $\mathcal{S}_{\text{HM}}$ .

$$\Delta\mathcal{S}_{\text{HM-IRT}} = \mathcal{S}_{\text{HM}} - \mathcal{S}_{\text{IRT}} = 0, \quad (4.3)$$

where  $\mathcal{S}_{\text{HM}}$  and  $\mathcal{S}_{\text{IRT}}$  are given in eq.(3.13) and eq.(3.31).

The regularized entanglement entropy corresponding to the HM and IRT surfaces are plotted in Fig.7(b).  $\mathcal{S}_{\text{HM}}$  (green line) starts from a finite value at  $t = t_b$  and increases. It dominates until  $t - t_b = t_{\text{HM-IRT}} \simeq 15.95$  when the phase transition between  $\mathcal{S}_{\text{HM}}$  and  $\mathcal{S}_{\text{IRT}}$  takes place, then  $\mathcal{S}_{\text{IRT}}$  will dominate for  $t - t_b > t_{\text{HM-IRT}}$ .

Finally, there is also a phase transition between  $\mathcal{S}_{\text{BRT}}$  and  $\mathcal{S}_{\text{HM}}$  that can be obtained from

$$\Delta\mathcal{S}_{\text{BRT-HM}} = \mathcal{S}_{\text{BRT}} - \mathcal{S}_{\text{HM}} = 0, \quad (4.4)$$

where  $\mathcal{S}_{\text{BRT}}$  and  $\mathcal{S}_{\text{HM}}$  are given in eq.(3.23) and eq.(3.13).

The regularized entanglement entropy corresponding to the BRT and HM surfaces are plotted in Fig.7(c). Both  $\mathcal{S}_{\text{BRT}}$  and  $\mathcal{S}_{\text{HM}}$  increases with time. Among the two,  $\mathcal{S}_{\text{BRT}}$  dominates until  $t - t_b = t_{\text{BRT-HM}} \simeq 6.47$  when the phase transition between  $\mathcal{S}_{\text{BRT}}$  and  $\mathcal{S}_{\text{HM}}$  takes place, then  $\mathcal{S}_{\text{HM}}$  will dominate for  $t - t_b > t_{\text{BRT-HM}}$ .

We have obtained the phase transitions of every pair of the three entanglement entropies corresponding to the BRT, HM, and IRT surfaces for the black hole horizon  $z_h = 10$  or  $T = 0.032$ . Now we put them together in Fig.8(a) with the red/green/blue line representing  $\mathcal{S}_{\text{BRT}}/\mathcal{S}_{\text{HM}}/\mathcal{S}_{\text{IRT}}$ . The three critical points are labeled by black, orange, and violet dots.

At early times,  $\mathcal{S}_{\text{BRT}}$  dominates the system. Later on, at  $t - t_b \simeq 6.47$ , the phase transition between  $\mathcal{S}_{\text{BRT}}$  and  $\mathcal{S}_{\text{HM}}$  takes place, and  $\mathcal{S}_{\text{HM}}$  becomes dominant. Then, at  $t - t_b \simeq 15.95$ , the phase transition between  $\mathcal{S}_{\text{HM}}$  and  $\mathcal{S}_{\text{IRT}}$  occurs, and  $\mathcal{S}_{\text{IRT}}$  becomes dominant. In addition, there is another phase transition between  $\mathcal{S}_{\text{BRT}}$  and  $\mathcal{S}_{\text{IRT}}$  that occurs between the above two phase transitions at

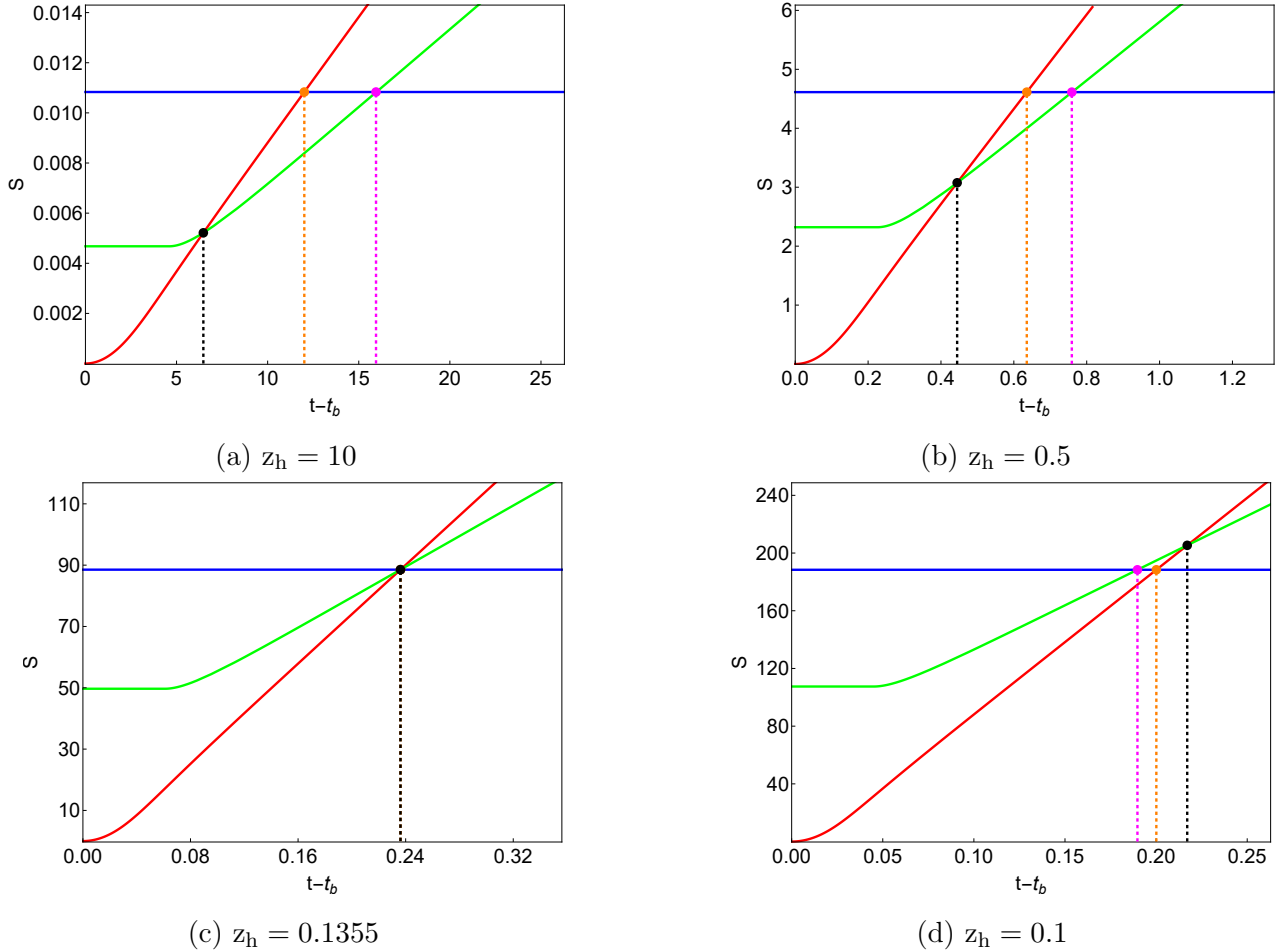


**Figure 8:** The behavior of the entanglement entropies,  $\mathcal{S}_{\text{BRT}}$  (red),  $\mathcal{S}_{\text{HM}}$  (green), and  $\mathcal{S}_{\text{IRT}}$  (blue), at different temperatures or black hole horizons. The black, orange, and violet dots indicate the phase transitions of  $\mathcal{S}_{\text{BRT}} \sim \mathcal{S}_{\text{HM}}$ ,  $\mathcal{S}_{\text{BRT}} \sim \mathcal{S}_{\text{IRT}}$ , and  $\mathcal{S}_{\text{HM}} \sim \mathcal{S}_{\text{IRT}}$ , respectively.

$t - t_b \simeq 12.01$ . However, this phase transition is irrelevant since it will not occur in the real physical process as shown in Fig.8(a).

Having obtained the phase diagram of the entanglement entropy at  $z_h = 10$  or  $T = 0.032$ , let us consider the phase diagrams at other temperatures. Fig.8(b) shows the entanglement entropies for the black hole horizon  $z_h = 0.5$ , which corresponds to a higher temperature  $T = 0.637$ . As in the case of  $z_h = 10$ , there are three phase transitions in this case. The phase transitions of  $\mathcal{S}_{\text{BRT}} \sim \mathcal{S}_{\text{HM}}$ ,  $\mathcal{S}_{\text{BRT}} \sim \mathcal{S}_{\text{IRT}}$ , and  $\mathcal{S}_{\text{HM}} \sim \mathcal{S}_{\text{IRT}}$  takes place at  $t - t_b \simeq 0.444$ ,  $t - t_b \simeq 0.636$  and  $t - t_b \simeq 0.759$ , respectively.

The phase structure for  $z_h = 0.5$  is similar to that for  $z_h = 10$ . Nevertheless, we have an important observation that the three critical points become closer for a smaller horizon or a higher

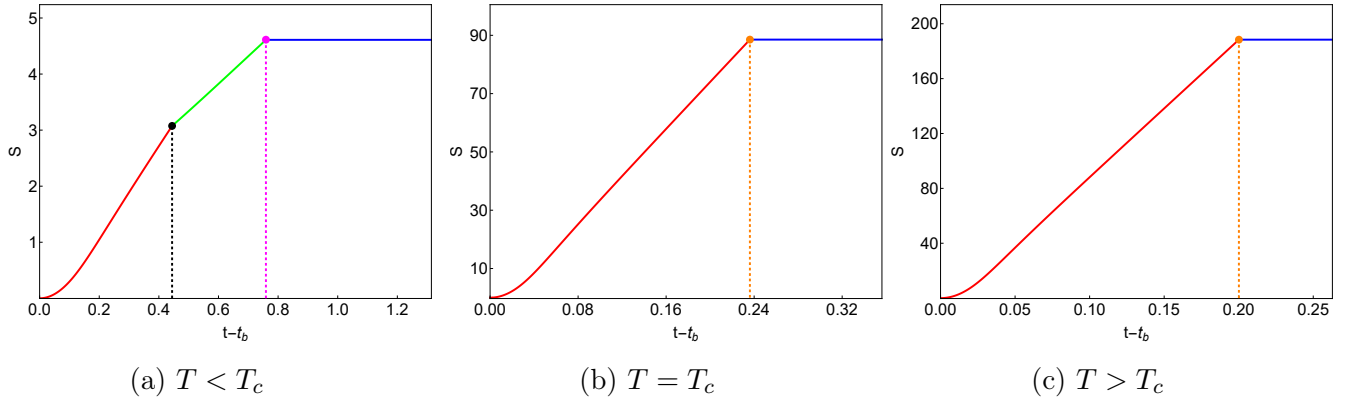


**Figure 9:** The Page curve for different temperatures. (a) For the case of  $z_h = 0.5$ ,  $\mathcal{S}_{\text{BRT}}$  transitions to  $\mathcal{S}_{\text{HM}}$  at  $t - t_b \simeq 0.444$ , then to  $\mathcal{S}_{\text{IRT}}$  at  $t - t_b \simeq 0.759$ . (b) For the case of  $z_h = 0.1355$ ,  $\mathcal{S}_{\text{BRT}}$  transitions directly to  $\mathcal{S}_{\text{IRT}}$  at  $t - t_b \simeq 0.236$ . (c) For the case of  $z_h = 0.1$ ,  $\mathcal{S}_{\text{BRT}}$  transitions directly to  $\mathcal{S}_{\text{IRT}}$  at  $t - t_b \simeq 0.200$ .

temperature, so that the duration of  $\mathcal{S}_{\text{HM}}$  domination shrinks. Therefore, an interesting question is whether or not the duration of  $\mathcal{S}_{\text{HM}}$  would shrink to zero if the temperature continuously increases? We found that the answer is yes.

Fig.8(c) shows the entanglement entropies for the black hole horizon  $z_h = 0.1355$ , which corresponds to the critical temperature  $T_c = 2.349$ . At this temperature, the three phase transitions coincide at the same point at  $t - t_b \simeq 0.236$  when the time duration of  $\mathcal{S}_{\text{HM}}$  shrinks to zero, and  $\mathcal{S}_{\text{BRT}}$  transit to  $\mathcal{S}_{\text{IRT}}$  directly at this critical point.

For  $T \geq T_c$ , for example, in the case of the black hole horizon  $z_h = 0.1$ , which corresponds to the temperature  $T = 3.183 \geq T_c$ , the entanglement entropies are shown in Fig.8(d). The phase transitions of  $\mathcal{S}_{\text{BRT}} \sim \mathcal{S}_{\text{HM}}$ ,  $\mathcal{S}_{\text{BRT}} \sim \mathcal{S}_{\text{IRT}}$ , and  $\mathcal{S}_{\text{HM}} \sim \mathcal{S}_{\text{IRT}}$  take place at  $t - t_b \simeq 0.217$ ,  $t - t_b \simeq 0.200$  and  $t - t_b \simeq 0.190$ , respectively. We notice that the order of the three phase transitions reverses. Because the phase transition between  $\mathcal{S}_{\text{BRT}}$  and  $\mathcal{S}_{\text{HM}}$  occurs after that between  $\mathcal{S}_{\text{BRT}}$  and  $\mathcal{S}_{\text{IRT}}$ , the dominant entanglement entropy  $\mathcal{S}_{\text{BRT}}$  will transit directly to  $\mathcal{S}_{\text{IRT}}$ .

## 4.2 Page Curve

Now we are ready to plot the Page curve from the phase transitions among the three RT surfaces obtained in section 4.1. The Page curves for different temperatures are plotted in Fig.9.

At low temperature  $T < T_c$ , e.g.  $z_h = 0.5$  or  $T = 0.637$ , the Page curve is plotted in Fig.9(a). At early times, the entanglement entropy is dominated by  $\mathcal{S}_{\text{BRT}}$  which increases from zero at  $t = t_b$ . After the first phase transition between  $\mathcal{S}_{\text{BRT}}$  and  $\mathcal{S}_{\text{HM}}$  takes place at  $t - t_b \simeq 0.444$ ,  $\mathcal{S}_{\text{HM}}$  becomes dominant until the second phase transition between  $\mathcal{S}_{\text{HM}}$  and  $\mathcal{S}_{\text{IRT}}$  takes place at  $t - t_b \simeq 0.759$

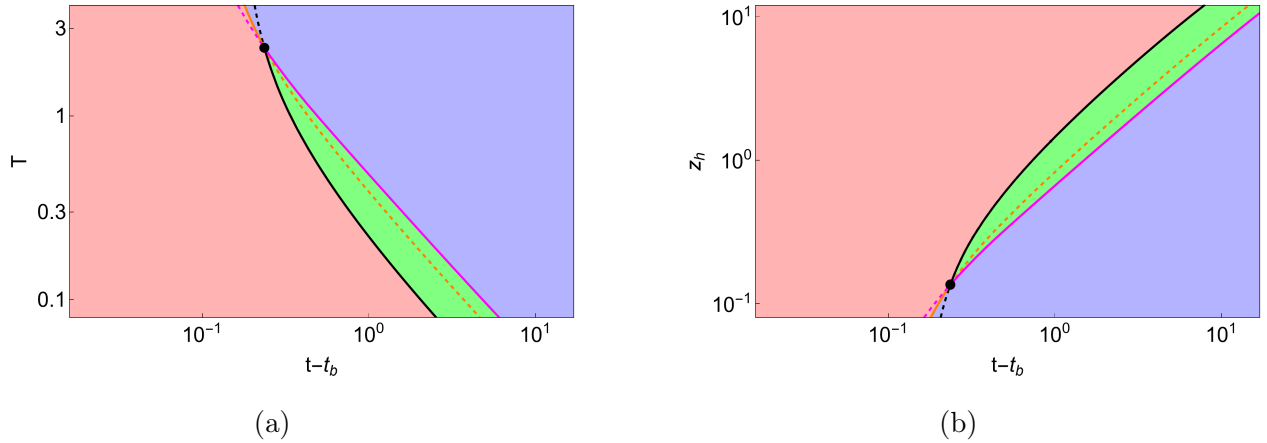


**Figure 10:** Phase diagram of the Hawking radiation entanglement entropy. The red/green/blue region represents the region where  $\mathcal{S}_{\text{BRT}}/\mathcal{S}_{\text{HM}}/\mathcal{S}_{\text{IERT}}$  dominates. The black, orange, and violet lines represent the phase transitions of  $\mathcal{S}_{\text{BRT}} \sim \mathcal{S}_{\text{HM}}$ ,  $\mathcal{S}_{\text{BRT}} \sim \mathcal{S}_{\text{IERT}}$ , and  $\mathcal{S}_{\text{HM}} \sim \mathcal{S}_{\text{IERT}}$ . The dashed parts do not occur in the real physical process. The black dot labels the triple point where the three phases meet together. (a) Phase diagram in the temperature  $T$  and time  $t - t_b$  plane. (b) Phase diagram in the black hole horizon  $z_h$  and time  $t - t_b$  plane.

when  $\mathcal{S}_{\text{IERT}}$  becomes dominant. In this case, the Page time is determined by the phase transition between  $\mathcal{S}_{\text{HM}}$  and  $\mathcal{S}_{\text{IERT}}$  labeled by the violet dot.

As the temperature grows, the duration of  $\mathcal{S}_{\text{HM}}$  shrinks. At the critical temperature  $T_c = 2.349$  or  $z_h = 0.1355$ , the Page curve is plotted in Fig.9(b). The contribution from the HM surface completely vanishes, and  $\mathcal{S}_{\text{BRT}}$  transits to  $\mathcal{S}_{\text{IERT}}$  directly. The Page time now is determined by the phase transition between  $\mathcal{S}_{\text{BRT}}$  and  $\mathcal{S}_{\text{IERT}}$  labeled by the orange dot.

As we go beyond the critical temperature as shown in Fig.9(c) for the case of  $T = 3.183$  or  $z_h = 0.1$ ,  $\mathcal{S}_{\text{BRT}}$  always transits to  $\mathcal{S}_{\text{IERT}}$  directly. The other two phase transitions are irrelevant. The Page time is determined by the phase transition between  $\mathcal{S}_{\text{BRT}}$  and  $\mathcal{S}_{\text{IERT}}$  labeled by the orange dot.

We conclude that the Page time decreases as the temperature grows. Among the three RT surfaces, only the IERT surface intersects with the Planck brane, and its entanglement wedge includes the interior of the eternal black hole. According to the entanglement wedge reconstruction, we can reconstruct the interior of the black hole when  $\mathcal{S}_{\text{IERT}}$  is dominant. The decreasing of the Page time as the temperature is growing implies that one can reconstruct the interior of the black hole earlier for a higher temperature black hole. This is consistent with the intuitive expectations since higher temperature black holes evaporate faster.

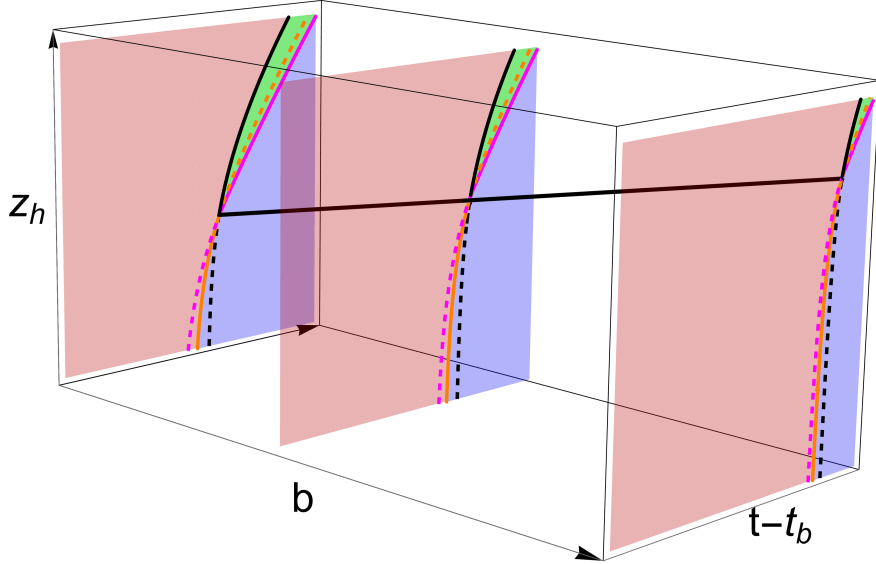


**Figure 11:** Different slices of the phase diagram as the cutoff  $b$  is varied.

### 4.3 Phase Diagram

The phase diagram in the temperature vs. time plane is plotted in Fig.10(a). The red region in the lower left part is dominated by  $\mathcal{S}_{\text{BRT}}$ , the blue region in the upper right part is dominated by  $\mathcal{S}_{\text{IRT}}$ , and the green region in between is dominated by  $\mathcal{S}_{\text{HM}}$ . The black, orange, and violet lines are the phase boundaries between different phases. The solid parts represent the phase boundaries in the real physical process. There is a triple point at  $T_c = 2.349$  and  $t - t_b = 0.236$  labeled by a black dot, where the three phases meet together. Below the critical temperature  $T_c$ , the system undergoes three phases,  $\mathcal{S}_{\text{BRT}}$ ,  $\mathcal{S}_{\text{HM}}$  and  $\mathcal{S}_{\text{IRT}}$  as time evolves, with the violet line indicating the Page time. While above the critical temperature, the system undergoes only two phases,  $\mathcal{S}_{\text{BRT}}$  and  $\mathcal{S}_{\text{IRT}}$ , with the orange line indicating the Page time.

This behavior of the phase diagram is consistent with our intuitive expectation: as the temperature grows, it becomes "easier" to decode the information inside the black hole due to the earlier Page time since the black hole radiates faster at higher temperatures.

So far we have only considered the system with a fixed cutoff  $b = 0.1$ . In the following, we will show how the phase diagram is affected by the variation of the cutoff. By using the simple relation

in eq.(2.14), the phase diagram can be plotted in the black hole horizon vs. time plane in Fig.10(b), which will be used to illustrate the effect from varying the cutoff  $b$ .

The phase diagrams in the black hole horizon vs. time plane for three different cutoffs are plotted in Fig.11. We can see that, as the cutoff  $b$  increases, the triple point moves to a new location with a larger black hole horizon (or lower temperature) and a later Page time. Remarkably, numerical calculations show that the path of the triple point is a straight line shown as the black line in Fig.11. However, the physical interpretation of this linear behavior of the triple point is not obvious to us and we will investigate it in the future.

## 5 Conclusion

In this work, we studied the entanglement entropy for a  $(d+1)$ -dimensional two-sided eternal black hole. We calculated the bulk entropy in the generalized entanglement entropy eq.(2.5) by doubly holographic correspondence. Our concrete setup is given by a black hole solution in a holographic BCFT as discussed in section 2.3.

In our setup, we introduced an ETW brane which is the hypersurface of the earliest Hawking radiation. The ETW brane moves away at the speed of light  $L = b + c(t - t_b)$ , and it defines a time-dependent effective radiation region  $[b_L, L] \cup [b_R, L]$ .

There are three RT surfaces associated with the bulk entropy. One is the HM surface which penetrates the horizon and connects the cutoffs  $b_L$  and  $b_R$  directly. The HM surface increases with time due to the stretching of the interior of the black hole. The second one is the BRT surface which intersects the ETW brane. The BRT surface increases with time due to the movement of the ETW brane. The last one is the IRT surface which intersects the Planck brane and supports an island. The IRT surface is a time-independent constant.

We investigated the phase transitions between every pair among the three RT surfaces in section 4.1. The phase transition time for each pair of the RT surfaces was determined by comparing their corresponding entanglement entropies. Putting all phase transitions together, we obtained the phase diagram of the entanglement entropy as shown in Fig.10.

We found a critical temperature  $T_c \simeq 2.394$  for the Page curve with  $b = 0.1$ . When the temperature is lower than the critical temperature, i.e.  $T < T_c$ , there are three durations for the entanglement entropy as shown in Fig.9(a).  $\mathcal{S}_{\text{BRT}}$  starts from zero at the initial time  $t = t_b$  and increases until the first phase transition, when  $\mathcal{S}_{\text{HM}}$  takes over and continuously increases. After the second phase transition,  $\mathcal{S}_{\text{IRT}}$  becomes dominant and keeps as a constant. On the other hand, when the temperature is higher than the critical temperature, i.e.  $T \geq T_c$ , the duration of  $\mathcal{S}_{\text{HM}}$  disappears, and  $\mathcal{S}_{\text{BRT}}$  transits to  $\mathcal{S}_{\text{IRT}}$  directly as shown in Fig.9(b,c).

## Acknowledgements

This work is supported by the Ministry of Science and Technology (MOST 109-2112-M-009-005) and National Center for Theoretical Science, Taiwan.

## References

- [1] S. W. Hawking. Particle Creation by Black Holes. *Commun. Math. Phys.*, 43:199–220, 1975. [Erratum: Commun.Math.Phys. 46, 206 (1976)].
- [2] S. W. Hawking. Black Holes and Thermodynamics. *Phys. Rev. D*, 13:191–197, 1976.
- [3] Don N. Page. Information in black hole radiation. *Phys. Rev. Lett.*, 71:3743–3746, 1993.
- [4] Ahmed Almheiri, Donald Marolf, Joseph Polchinski, and James Sully. Black Holes: Complementarity or Firewalls? *JHEP*, 02:062, 2013.
- [5] Kyriakos Papadodimas and Suvrat Raju. An Infalling Observer in AdS/CFT. *JHEP*, 10:212, 2013.
- [6] Daniel Harlow and Patrick Hayden. Quantum Computation vs. Firewalls. *JHEP*, 06:085, 2013.
- [7] Ahmed Almheiri, Donald Marolf, Joseph Polchinski, Douglas Stanford, and James Sully. An Apologia for Firewalls. *JHEP*, 09:018, 2013.
- [8] Juan Maldacena and Leonard Susskind. Cool horizons for entangled black holes. *Fortsch. Phys.*, 61:781–811, 2013.
- [9] Seth Lloyd and John Preskill. Unitarity of black hole evaporation in final-state projection models. *JHEP*, 08:126, 2014.
- [10] Kyriakos Papadodimas and Suvrat Raju. Black Hole Interior in the Holographic Correspondence and the Information Paradox. *Phys. Rev. Lett.*, 112(5):051301, 2014.
- [11] Ning Bao, Adam Bouland, Aidan Chatwin-Davies, Jason Pollack, and Henry Yuen. Rescuing Complementarity With Little Drama. *JHEP*, 12:026, 2016.
- [12] Ning Bao, Sean M. Carroll, Aidan Chatwin-Davies, Jason Pollack, and Grant N. Remmen. Branches of the Black Hole Wave Function Need Not Contain Firewalls. *Phys. Rev. D*, 97(12):126014, 2018.
- [13] J. D. Bekenstein. Black holes and the second law. *Lett. Nuovo Cim.*, 4:737–740, 1972.
- [14] Jacob D. Bekenstein. Black holes and entropy. *Phys. Rev. D*, 7:2333–2346, 1973.
- [15] Shinsei Ryu and Tadashi Takayanagi. Holographic derivation of entanglement entropy from AdS/CFT. *Phys. Rev. Lett.*, 96:181602, 2006.
- [16] Shinsei Ryu and Tadashi Takayanagi. Aspects of Holographic Entanglement Entropy. *JHEP*, 08:045, 2006.

- [17] Veronika E. Hubeny, Mukund Rangamani, and Tadashi Takayanagi. A Covariant holographic entanglement entropy proposal. *JHEP*, 07:062, 2007.
- [18] Thomas Faulkner, Aitor Lewkowycz, and Juan Maldacena. Quantum corrections to holographic entanglement entropy. *JHEP*, 11:074, 2013.
- [19] Netta Engelhardt and Aron C. Wall. Quantum Extremal Surfaces: Holographic Entanglement Entropy beyond the Classical Regime. *JHEP*, 01:073, 2015.
- [20] Netta Engelhardt and Sebastian Fischetti. Surface Theory: the Classical, the Quantum, and the Holographic. *Class. Quant. Grav.*, 36(20):205002, 2019.
- [21] Xi Dong, Daniel Harlow, and Aron C. Wall. Reconstruction of Bulk Operators within the Entanglement Wedge in Gauge-Gravity Duality. *Phys. Rev. Lett.*, 117(2):021601, 2016.
- [22] Geoffrey Penington. Entanglement Wedge Reconstruction and the Information Paradox. *JHEP*, 09:002, 2020.
- [23] Ahmed Almheiri, Netta Engelhardt, Donald Marolf, and Henry Maxfield. The entropy of bulk quantum fields and the entanglement wedge of an evaporating black hole. *JHEP*, 12:063, 2019.
- [24] Ahmed Almheiri, Raghu Mahajan, Juan Maldacena, and Ying Zhao. The Page curve of Hawking radiation from semiclassical geometry. *JHEP*, 03:149, 2020.
- [25] Hong Zhe Chen, Zachary Fisher, Juan Hernandez, Robert C. Myers, and Shan-Ming Ruan. Information Flow in Black Hole Evaporation. *JHEP*, 03:152, 2020.
- [26] Ahmed Almheiri, Raghu Mahajan, and Juan Maldacena. Islands outside the horizon. 10 2019.
- [27] Friðrik Freyr Gautason, Lukas Schneiderbauer, Watse Sybesma, and Lárus Thorlacius. Page Curve for an Evaporating Black Hole. *JHEP*, 05:091, 2020.
- [28] Takanori Anegawa and Norihiro Iizuka. Notes on islands in asymptotically flat 2d dilaton black holes. *JHEP*, 07:036, 2020.
- [29] Vijay Balasubramanian, Ben Craps, Mikhail Khramtsov, and Edgar Shaghoulian. Submerging islands through thermalization. *JHEP*, 10:048, 2021.
- [30] Moshe Rozali, James Sully, Mark Van Raamsdonk, Christopher Waddell, and David Wakeham. Information radiation in BCFT models of black holes. *JHEP*, 05:004, 2020.
- [31] Ahmed Almheiri, Raghu Mahajan, and Jorge E. Santos. Entanglement islands in higher dimensions. *SciPost Phys.*, 9(1):001, 2020.
- [32] Koji Hashimoto, Norihiro Iizuka, and Yoshinori Matsuo. Islands in Schwarzschild black holes. *JHEP*, 06:085, 2020.
- [33] Mohsen Alishahiha, Amin Faraji Astaneh, and Ali Naseh. Island in the presence of higher derivative terms. *JHEP*, 02:035, 2021.

- [34] Hao Geng and Andreas Karch. Massive islands. *JHEP*, 09:121, 2020.
- [35] Hong Zhe Chen, Robert C. Myers, Dominik Neuenfeld, Ignacio A. Reyes, and Joshua Sandor. Quantum Extremal Islands Made Easy, Part I: Entanglement on the Brane. *JHEP*, 10:166, 2020.
- [36] Venkatesa Chandrasekaran, Masamichi Miyaji, and Pratik Rath. Including contributions from entanglement islands to the reflected entropy. *Phys. Rev. D*, 102(8):086009, 2020.
- [37] Dongsu Bak, Chanju Kim, Sang-Heon Yi, and Junggi Yoon. Unitarity of entanglement and islands in two-sided Janus black holes. *JHEP*, 01:155, 2021.
- [38] Raphael Bousso and Elizabeth Woldenhain. Gravity/ensemble duality. *Phys. Rev. D*, 102(6):066005, 2020.
- [39] Chethan Krishnan. Critical Islands. *JHEP*, 01:179, 2021.
- [40] Roberto Emparan, Antonia Micol Frassino, and Benson Way. Quantum BTZ black hole. *JHEP*, 11:137, 2020.
- [41] Hong Zhe Chen, Robert C. Myers, Dominik Neuenfeld, Ignacio A. Reyes, and Joshua Sandor. Quantum Extremal Islands Made Easy, Part II: Black Holes on the Brane. *JHEP*, 12:025, 2020.
- [42] Yi Ling, Yuxuan Liu, and Zhuo-Yu Xian. Island in Charged Black Holes. *JHEP*, 03:251, 2021.
- [43] Aranya Bhattacharya, Anindya Chanda, Sabyasachi Maulik, Christian Northe, and Shibaji Roy. Topological shadows and complexity of islands in multiboundary wormholes. *JHEP*, 02:152, 2021.
- [44] Juan Hernandez, Robert C. Myers, and Shan-Ming Ruan. Quantum extremal islands made easy. Part III. Complexity on the brane. *JHEP*, 02:173, 2021.
- [45] Jaydeep Kumar Basak, Debarshi Basu, Vinay Malvimat, Himanshu Parihar, and Gautam Sengupta. Islands for Entanglement Negativity. 12 2020.
- [46] Elena Caceres, Arnab Kundu, Ayan K. Patra, and Sanjit Shashi. Warped Information and Entanglement Islands in AdS/WCFT. *JHEP*, 07:004, 2021.
- [47] Feiyu Deng, Jinwei Chu, and Yang Zhou. Defect extremal surface as the holographic counterpart of Island formula. *JHEP*, 03:008, 2021.
- [48] Anna Karlsson. Concerns about the replica wormhole derivation of the island conjecture. 1 2021.
- [49] Rong-Xin Miao. Codimension-n holography for cones. *Phys. Rev. D*, 104(8):086031, 2021.
- [50] Constantin Bachas and Vassilis Papadopoulos. Phases of Holographic Interfaces. *JHEP*, 04:262, 2021.
- [51] Alex May and David Wakeham. Quantum tasks require islands on the brane. *Class. Quant. Grav.*, 38(14):144001, 2021.
- [52] Kohki Kawabata, Tatsuma Nishioka, Yoshitaka Okuyama, and Kento Watanabe. Probing Hawking radiation through capacity of entanglement. *JHEP*, 05:062, 2021.

[53] Aranya Bhattacharya, Arpan Bhattacharyya, Pratik Nandy, and Ayan K. Patra. Islands and complexity of eternal black hole and radiation subsystems for a doubly holographic model. *JHEP*, 05:135, 2021.

[54] Wontae Kim and Mungon Nam. Entanglement entropy of asymptotically flat non-extremal and extremal black holes with an island. *Eur. Phys. J. C*, 81(10):869, 2021.

[55] Lars Aalsma and Watse Sybesma. The Price of Curiosity: Information Recovery in de Sitter Space. *JHEP*, 05:291, 2021.

[56] Dominik Neuenfeld. The Dictionary for Double Holography and Graviton Masses in d Dimensions. 4 2021.

[57] Hao Geng, Severin Lüst, Rashmish K. Mishra, and David Wakeham. Holographic BCFTs and Communicating Black Holes. *jhep*, 08:003, 2021.

[58] Vijay Balasubramanian, Arjun Kar, and Tomonori Ugajin. Entanglement between two gravitating universes. 4 2021.

[59] Christoph F. Uhlemann. Islands and Page curves in 4d from Type IIB. *JHEP*, 08:104, 2021.

[60] Dominik Neuenfeld. Double Holography as a Model for Black Hole Complementarity. 5 2021.

[61] Kohki Kawabata, Tatsuma Nishioka, Yoshitaka Okuyama, and Kento Watanabe. Replica wormholes and capacity of entanglement. *JHEP*, 10:227, 2021.

[62] Jinwei Chu, Feiyu Deng, and Yang Zhou. Page curve from defect extremal surface and island in higher dimensions. *JHEP*, 10:149, 2021.

[63] Yizhou Lu and Jiong Lin. Islands in Kaluza-Klein black holes. 6 2021.

[64] Jorrit Kruthoff, Raghu Mahajan, and Chitraang Murdia. Free fermion entanglement with a semitransparent interface: the effect of graybody factors on entanglement islands. *SciPost Phys.*, 11:063, 2021.

[65] Ibrahim Akal, Yuya Kusuki, Noburo Shiba, Tadashi Takayanagi, and Zixia Wei. Holographic moving mirrors. *Class. Quant. Grav.*, 38(22):224001, 2021.

[66] Jaydeep Kumar Basak, Debarshi Basu, Vinay Malvimat, Himanshu Parihar, and Gautam Sengupta. Page Curve for Entanglement Negativity through Geometric Evaporation. 6 2021.

[67] Elena Caceres, Arnab Kundu, Ayan K. Patra, and Sanjit Shashi. Page Curves and Bath Deformations. 6 2021.

[68] Hidetoshi Omiya and Zixia Wei. Causal Structures and Nonlocality in Double Holography. 7 2021.

[69] Hao Geng, Andreas Karch, Carlos Perez-Pardavila, Suvrat Raju, Lisa Randall, Marcos Riojas, and Sanjit Shashi. Inconsistency of Islands in Theories with Long-Range Gravity. 7 2021.

[70] Hong Zhe Chen, Zachary Fisher, Juan Hernandez, Robert C. Myers, and Shan-Ming Ruan. Evaporating Black Holes Coupled to a Thermal Bath. *JHEP*, 01:065, 2021.

[71] D. M. McAvity and H. Osborn. Conformal field theories near a boundary in general dimensions. *Nucl. Phys. B*, 455:522–576, 1995.

[72] Andreas Karch and Lisa Randall. Locally localized gravity. *JHEP*, 05:008, 2001.

[73] Oliver DeWolfe, Daniel Z. Freedman, and Hirosi Ooguri. Holography and defect conformal field theories. *Phys. Rev. D*, 66:025009, 2002.

[74] Tadashi Takayanagi. Holographic Dual of BCFT. *Phys. Rev. Lett.*, 107:101602, 2011.

[75] Mitsutoshi Fujita, Tadashi Takayanagi, and Erik Tonni. Aspects of AdS/BCFT. *JHEP*, 11:043, 2011.

[76] Masahiro Nozaki, Tadashi Takayanagi, and Tomonori Ugajin. Central Charges for BCFTs and Holography. *JHEP*, 06:066, 2012.

[77] Juan Martin Maldacena. The Large N limit of superconformal field theories and supergravity. *Adv. Theor. Math. Phys.*, 2:231–252, 1998.

[78] Edward Witten. Anti-de Sitter space and holography. *Adv. Theor. Math. Phys.*, 2:253–291, 1998.

[79] Thomas Hartman and Juan Maldacena. Time Evolution of Entanglement Entropy from Black Hole Interiors. *JHEP*, 05:014, 2013.

[80] Lisa Randall and Raman Sundrum. A Large mass hierarchy from a small extra dimension. *Phys. Rev. Lett.*, 83:3370–3373, 1999.

[81] Lisa Randall and Raman Sundrum. An Alternative to compactification. *Phys. Rev. Lett.*, 83:4690–4693, 1999.

[82] Andreas Karch and Lisa Randall. Open and closed string interpretation of SUSY CFT’s on branes with boundaries. *JHEP*, 06:063, 2001.

[83] Massimo Porrati. Mass and gauge invariance 4. Holography for the Karch-Randall model. *Phys. Rev. D*, 65:044015, 2002.

[84] Andreas Karch, Emanuel Katz, and Lisa Randall. Absence of a VVDZ discontinuity in AdS(AdS). *JHEP*, 12:016, 2001.

[85] M. Porrati. Higgs phenomenon for 4-D gravity in anti-de Sitter space. *JHEP*, 04:058, 2002.

[86] Massimo Porrati and Andrei Starinets. On the graviton selfenergy in AdS(4). *Phys. Lett. B*, 532:48–54, 2002.

[87] M. J. Duff, James T. Liu, and H. Sati. Complementarity of the Maldacena and Karch-Randall pictures. *Phys. Rev. D*, 69:085012, 2004.

- [88] Ofer Aharony, Adam B. Clark, and Andreas Karch. The CFT/AdS correspondence, massive gravitons and a connectivity index conjecture. *Phys. Rev. D*, 74:086006, 2006.
- [89] En-Jui Chang, Chia-Jui Chou, and Yi Yang. Holographic entanglement entropy in boundary conformal field theory. *Phys. Rev. D*, 98(10):106016, 2018.
- [90] Rong-Xin Miao, Chong-Sun Chu, and Wu-Zhong Guo. New proposal for a holographic boundary conformal field theory. *Phys. Rev. D*, 96(4):046005, 2017.
- [91] Chong-Sun Chu, Rong-Xin Miao, and Wu-Zhong Guo. On New Proposal for Holographic BCFT. *JHEP*, 04:089, 2017.